Cell Death & Differentiation (2021) 28:1208–1221
https://doi.org/10.1038/s41418-020-00642-6

Cell Death & Differentiation

ARTICLE

Check for updates

Maternally inherited intron coordinates primordial germ cell homeostasis during *Drosophila* embryogenesis

Ismail Osman[1,2] · Jun Wei Pek[1,2]

Received: 8 May 2020 / Revised: 7 October 2020 / Accepted: 8 October 2020 / Published online: 22 October 2020

Abstract
Primordial germ cells (PGCs) give rise to the germline stem cells (GSCs) in the adult *Drosophila* gonads. Both PGCs and GSCs need to be tightly regulated to safeguard the survival of the entire species. During larval development, a non-cell autonomous homeostatic mechanism is in place to maintain PGC number in the gonads. Whether such germline homeostasis occurs during early embryogenesis before PGCs reach the gonads remains unclear. We have previously shown that the maternally deposited sisRNA *sisR-2* can influence GSC number in the female progeny. Here we uncover the presence of a homeostatic mechanism regulating PGCs during embryogenesis. *sisR-2* represses PGC number by promoting PGC death. Surprisingly, increasing maternal *sisR-2* leads to an increase in PGC death, but no drop in PGC number was observed. This is due to ectopic division of PGCs via the de-repression of Cyclin B, which is governed by a genetic pathway involving *sisR-2, bantam* and *brat*. We propose a cell autonomous model whereby germline homeostasis is achieved by preserving PGC number during embryogenesis.

Introduction

In sexually reproducing animals, germ cells give rise to the gametes, which carry genetic information to the next generation. As such, germ cells are often regarded as being immortal [1]. Hence, it is vital that germ cells are tightly regulated, both during development and adulthood, to safeguard the survival of the entire species.

In *Drosophila*, germ cells are generated in the developing embryo through a process known as preformation, via the inheritance of a specialized maternally provided cytoplasm termed the germplasm [2]. In the syncytial embryo, nuclei that migrate to the posterior pole will encounter the germplasm and cellularize to form primordial germ cells (PGCs) [3]. These PGCs proliferate asynchronously from the adjacent somatic cells, and by stage 5 of embryogenesis, cease their divisions to form the final pool of 30–40 PGCs [4]. During gastrulation, PGCs are initially passively brought into the embryo where they will begin their active migration towards the somatic gonadal precursors (SGPs) to form the embryonic gonads at stage 13 (Fig. 1a) [5]. Of the final pool of PGCs formed at stage 5, only a fraction of these PGCs successfully make it to the gonads [3]. Some of these PGCs die during their active migration whereas some mismigrate and eventually die [6–9]. Subsequently, during larval development, a homeostatic mechanism is in place to correct for any drop in the number of PGCs in the gonads [10]. Whether such PGC homeostasis occurs during early embryogenesis before they reach the gonads remains unclear.

Stable intronic sequence RNAs (sisRNAs) are proposed to function as an additional layer of gene regulation [11]. sisRNAs have been reported to participate in regulatory feedback loops to either enhance or repress gene expression, as well as acting as protein decoys to influence splicing of RNAs [12–15]. We previously characterized *sisR-2*, an ovary-enriched sisRNA that is maternally deposited into the oocytes [16]. We showed that *sisR-2* represses germline

Edited by G. Melino

Supplementary information The online version of this article (https://doi.org/10.1038/s41418-020-00642-6) contains supplementary material, which is available to authorized users.

✉ Jun Wei Pek
junwei@tll.org.sg

[1] Temasek Life Sciences Laboratory, 1 Research Link National University of Singapore, Singapore 117604, Singapore

[2] Department of Biological Sciences, National University of Singapore, Singapore 117543, Singapore

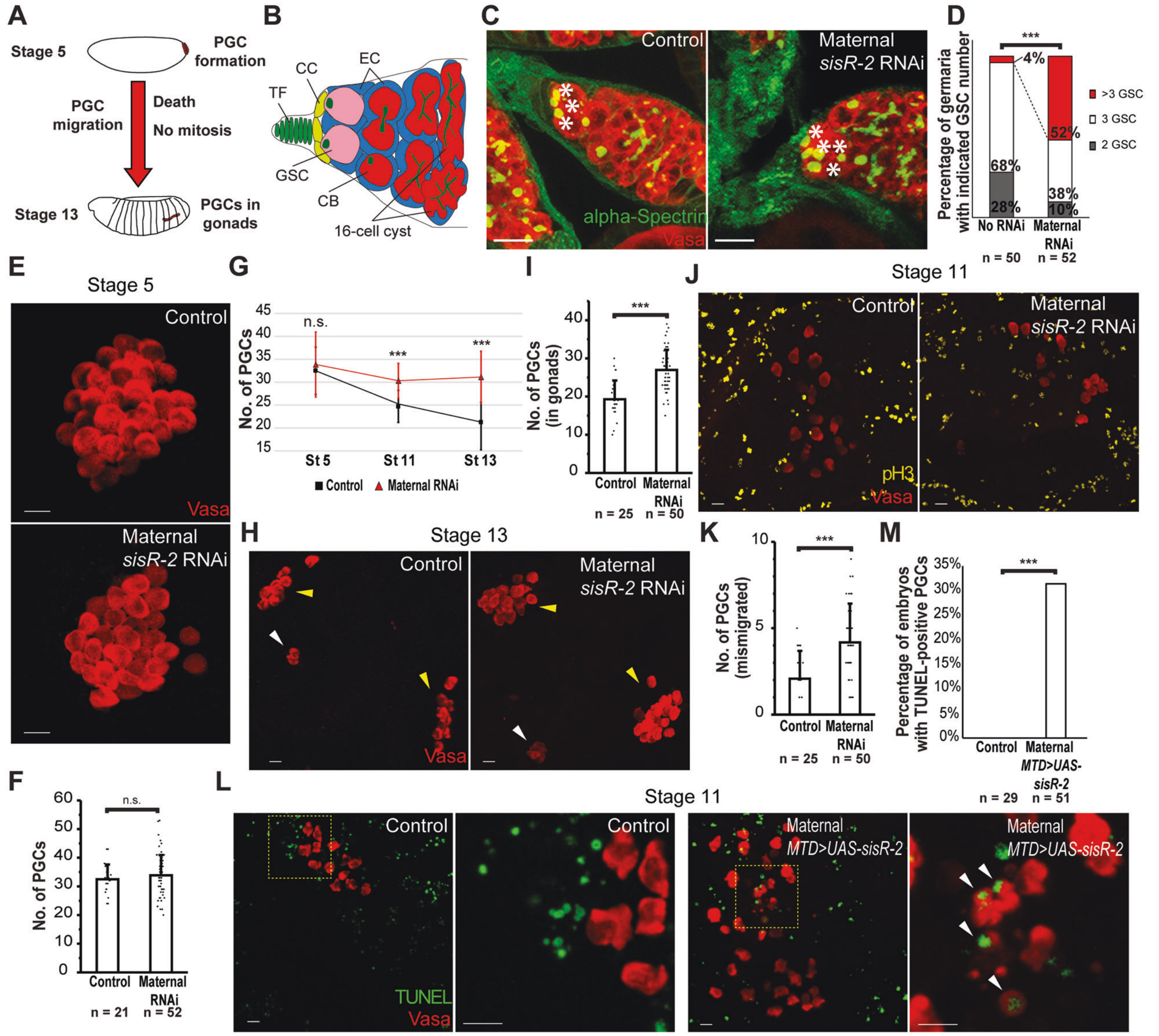

Fig. 1 Maternal *sisR-2* promotes PGC death. a Diagram highlighting key processes of PGC development during *Drosophila* embryogenesis. **b** Diagram showing the cell types in a *Drosophila* germarium in the ovary. TF terminal filament, CC cap cells, GSC germline stem cells, EC escort cells, CB cystoblasts. **c** Confocal images showing the germaria of the indicated genotypes stained with alpha-Spectrin (green) and Vasa (red). Control: *sisR-2* RNAi parental. Maternal *sisR-2* RNAi: *vasa-Gal4* driven RNAi. GSCs were marked by asterisks (*). **d** Chart showing the percentage of germaria with the indicated number of GSCs in different genotypes shown in **c**. ***$p <$ 0.001. Student's *t* test was performed, comparing the mean number of GSCs of the indicated genotypes. **e** Confocal images showing the PGCs in stage 5 embryos of the indicated genotypes stained with Vasa (red). Control: *sisR-2* RNAi parental. Maternal *sisR-2* RNAi: *vasa-Gal4* driven RNAi. **f** Chart showing the number of PGCs in different genotypes shown in **e**. Student's *t* test was performed, comparing the mean number of PGCs of the indicated genotypes. Error bars depict SD. **g** Chart showing the total number of PGCs in different genotypes in stage 5, 11 and 13 as shown in **e**, **h** and (S1B). ***$p < 0.001$. Student's *t* test was performed, comparing the mean number of PGCs of the indicated genotypes. Error bars depict SD. **h** Confocal images showing the PGCs in stage 13 embryos of the indicated genotypes stained with Vasa (red). Yellow arrowheads: PGCs in gonads. White arrowhead: mismigrated PGCs. Control: *sisR-2* RNAi parental. Maternal *sisR-2* RNAi: *vasa-Gal4* driven RNAi. **i** Chart showing the number of PGCs in the gonads of different genotypes shown in **h**. ***$p < 0.001$. Student's *t* test was performed, comparing the mean number of PGCs of the indicated genotypes. Error bars depict SD. **j** Confocal images showing the PGCs in stage 11 embryos of the indicated genotypes stained with Vasa (red) and pH3 (yellow). Control: *sisR-2* RNAi parental. Maternal *sisR-2* RNAi: *vasa-Gal4* driven RNAi. **k** Chart showing the number of mismigrated PGCs in the embryos of different genotypes shown in **h**. ***$p < 0.001$. Student's *t* test was performed, comparing the mean number of mismigrated PGCs of the indicated genotypes. Error bars depict SD. **l** Confocal images showing the PGCs in stage 11 embryos of the indicated genotypes stained with Vasa (red) and TUNEL (green). Panels on the right are magnified images of the dashed yellow box. White arrowhead: TUNEL-positive PGCs. Control: *y w*. **m** Chart showing the percentage of embryos with TUNEL-positive PGCs of different genotypes shown in **l**. ***$p < 0.001$. Fisher's exact test was performed, comparing the number of embryos with or without TUNEL-positive PGCs. Scale bar: 10 µm.

stem cell (GSC) number in the adult females via a lipid metabolism gene *dFAR1* [17]. In addition, we found that *sisR-2* is upregulated during starvation, which would lead to a loss of GSCs [17]. However, we discovered a negative feedback loop involving the miRNA *bantam*, which represses the activity of *sisR-2* [17]. As a result, this homeostatic mechanism prevents the loss of GSCs during starvation in *Drosophila* [17]. In addition, we found that maternally deposited *sisR-2* influenced the number of GSCs in the female progeny, however, the cellular and molecular mechanisms are still unknown.

Here, we study the function of *sisR-2* in PGC development and uncover the presence of a homeostatic mechanism regulating PGCs during embryogenesis. We found that *sisR-2* represses PGC number by promoting PGC death. Surprisingly, increasing the maternally deposited pool of *sisR-2* resulted in an increase in PGC death, but no apparent drop in PGC number. This is due to ectopic division of PGCs via the de-repression of Cyclin B, which is governed by a genetic pathway involving *sisR-2, bantam* and *brat*. Our study provides evidence for a mechanism that achieves germline homeostasis by preserving PGC number during embryogenesis.

Methods

Fly strains

Flies were maintained in standard cornmeal medium at 25 °C unless otherwise stated. The following Gal4 drivers were used to drive UAS-transgene expression in the germline: *MTD-Gal4* [18], *nanos-Gal4-VP16* [19], *vasa-Gal4* (gift from Y. Yamashita) and *NGT40-Gal4-VP16* [20]. *vasa-Gal4/CyO;sisR-2 RNAi-1* and *UAS-sisR-2* was generated previously [17, 21]. *UAS-bantam sponge*, *UAS-bantam*, and *UAS-bantam sensor* were gifts from Cohen [22, 23]. *brat[11]*, *UAS-brat*, and *UAS-brat[GD]* were gifts from Ashe [24]. *UAS-hid* (Bloomington #65408), *hid [05014]* (Bloomington #83349) and *TOR RNAi* (Bloomington #339510) were obtained from the Bloomington Stock Center. *dsRed*-intron-*myc* overexpression flies was generated as described previously [16]. Mutations were introduced into the *mbt* intron using the Q5 site-directed mutagenesis kit (New England Biolabs). Injection was carried out by BestGene Inc. Oligonucleotides sequences are available in Table S1. Starvation experiments were done as described previously [17]. For embryo collections, females and males of the indicated genotypes were crossed in cages with apple juice plates, supplemented with wet yeast paste. Embryos were collected hourly, and allowed to develop to the required embryonic stage at either 18 °C or 25 °C [25].

Immunostaining

Immunostaining of ovaries was performed as described previously [17]. Ovaries were fixed in a solution of 16% paraformaldehyde and Grace's medium at a ratio of 2:1 for 20 min, rinsed, and washed with PBX solution (PBS containing 0.2% Triton X-100) three times for 10 min each, and pre-absorbed for 30 min in PBX containing 5% normal goat serum. Ovaries were incubated overnight with primary antibodies at room temperature, washed three times for 20 min each with PBX before a 4 h incubation with secondary antibodies at room temperature. Ovaries were again washed three times for 20 min each with PBX. Staged embryos were dechorionated in 50% bleach (1:1, water:bleach) for 3 min and fixed in a scintillation vial containing heptane and fresh 4% paraformaldehyde in PBS with shaking for 20 min. Dechorionated fixed embryos were devitellinised in 1:3, heptane:methanol with vigorous shaking for 1 min. Devitellinised embryos were rinsed in methanol five times. Primary antibodies used in this study are as follows: guinea pig anti-Vasa (1:1000) [26], mouse monoclonal anti-a-Spectrin (3A9, 1:1; Developmental Studies Hybridoma Bank), mouse monoclonal anti-pH3 (ab14955, 1:200; Abcam), rabbit anti-Hid (gift from HD Ryoo) and mouse monoclonal anti-CyclinB (F2F4, undiluted; Developmental Studies Hybridoma Bank). For accurate counting of PGCs in stage 5 embryos, immunostained embryos were sliced using a sharp needle at the posterior end. Sliced embryo sections were mounted with the side containing PGCs facing the coverslip [7]. TUNEL assay was done using the In Situ Cell Death Detection Kit (Roche). Images were taken using Leica SPEII microscope and processed using either Adobe Photoshop, ImageJ or the Leica LAS X software.

Immunostaining signal quantification

Immunostaining of sample embryos were carried out in parallel. Images were taken under identical confocal settings and analyzed using ImageJ. PGCs were identified using Vasa staining. Anti-Hid, anti-Brat or anti-Cyclin-B fluorescence intensity was measured at three separate areas in the same cell, and an average was taken. Anti-Vasa fluorescence intensity was similarly measured at 3 separate areas in the same cell and used for normalization.

RNA extraction

RNA extraction was done as described previously [17]. Tissues were homogenized in 1.5 ml Eppendorf tubes using a plastic pestle and RNA was extracted using the TRIzol extraction protocol (Ambion) or the Direct-zol RNA miniprep kit (Zymo Research). RNA was quantified with the NanoDrop 2000 spectrophotometer (Thermo Scientific).

RT-PCR

For standard RT-PCR, total RNA was reverse transcribed with random hexamers or oligo-dT for 1 h using AMV-RT (New England Biolabs), M-MLV RT (Promega) or Superscript III (Invitrogen). PCR was carried out using the resulting cDNA. For qPCR, SYBR Fast qPCR kit master mix (2X) universal (Kapa Biosystems, USA) was used with addition of ROX reference dye high and carried out on the Applied Biosystems 7900HT Fast Real-Time PCR system. Oligonucleotides sequences are in Table S1 and reported previously [17].

Western blotting

Western blotting was performed as previously described [17]. Protein lysates were run on an SDS gel and transferred to a PVDF membrane. Antibodies used were mouse anti-GFP (1:1000; Invitrogen) and mouse anti-alpha Tubulin (1:10,000; Millipore). Western blot detection was done digitally using the ChemiDoc Touch Imaging System (BioRad) and under non-saturating conditions.

Statistics

In all experiments, the tests that were used and the number of independent biological replicates and gonads/embryos were indicated in the figure legends or figures. *P* values and definitions of error bars were indicated in the legends. Sample sizes were not pre-determined prior to the experiments. T-tests were performed on samples that are normally distributed.

Results

Maternal *sisR-2* promotes PGC death

We previously showed that reducing the levels of maternally deposited *sisR-2* led to more GSCs in the resulting female progeny dissected at day 8 [17]. Interestingly, the increase in number of GSCs was also observed in female flies dissected immediately after eclosion (Fig. 1b–d). Since GSCs are derived from the PGCs formed in the early embryos, and *sisR-2* is maternally deposited, we hypothesized that maternal *sisR-2* regulates PGCs during embryogenesis. First, to examine if *sisR-2* regulates the formation of PGCs, we counted the number of PGCs in stage 5 embryos with reduced maternally deposited *sisR-2* (hereafter referred to as *sisR-2* RNAi embryos) (Fig. S1A and S1B). We did not observe a change in the number of PGCs between controls and stage 5 *sisR-2* RNAi embryos (Fig. 1e–g), indicating that *sisR-2* does not regulate the formation of PGCs in the early embryos (Fig. 1a).

Next, to investigate if maternal *sisR-2* regulates the number of PGCs that reach the embryonic gonads, we counted the number of PGCs in stage 13 embryos (Fig. 1a). Interestingly, we observed a significant increase in the number of PGCs in the embryonic gonads of stage 13 *sisR-2* RNAi embryos as compared to the controls (19.8 ± 4.9 PGCs in controls vs. 27.0 ± 5.3 PGCs in *sisR-2* RNAi, yellow arrowheads) (Fig. 1g–i). Consistently, we also observed an increase in PGC number in stage 13 embryos with the same maternal *sisR-2* RNAi driven by another Gal4 driver (*MTD-Gal4*) (Fig. S1B–S1E). Moreover, this increase in PGC number was also observed in stage 11 embryos, when the PGCs are still actively migrating (24.7 ± 3.5 PGCs in controls vs. 30.3 ± 3.8 PGCs in *sisR-2* RNAi) (Figs. 1g, S1F, and S1G). PGCs do not undergo mitosis during these two stages although they are competent to divide (Fig. 1a) [4, 27]. Thus, we checked if the increase in the number of PGCs was due to premature proliferation by staining with a mitotic marker anti-phospho-Histone H3 (pH3). As expected, no pH3-positive PGCs were detected in the stage 11 control embryos ($n = 100$) (Fig. 1j). We did not observe any pH3-positive PGCs in stage 11 *sisR-2* RNAi embryos ($n = 100$), indicating that PGCs were not dividing (Fig. 1j). Moreover, we did not detect an increase in the mitotic cyclin Cyclin B in PGCs from sisR-2 RNAi embryos further confirming that the increase in PGCs in *sisR-2* RNAi embryos cannot be attributed to proliferation (Fig. S1H and S1I).

In *wunen* mutants, the number of PGCs that reach the embryonic gonads decreases due to a defect in PGC migration [9]. Since there was an increase in PGCs reaching the embryonic gonads in *sisR-2* RNAi embryos, we wondered if *sisR-2* represses PGC migration. We counted the number of mismigrated PGCs in stage 13 embryos and did not detect a decrease in mismigrated PGCs in *sisR-2* RNAi embryos as compared to controls (Fig. 1h, k, white arrowheads). Instead, we observed a slight but significant increase in mismigrated PGCs in *sisR-2* RNAi embryos (2.1 ± 1.6 PGCs in controls vs. 4.2 ± 2.2 PGCs in *sisR-2* RNAi (*vasa-Gal4*) and 6.5 ± 2.4 in *sisR-2* RNAi (*MTD-Gal4*)) (Figs. 1h, k, S1D and S1J). Thus, this observation rules out the possibility that the increase in PGCs observed in the embryonic gonads of *sisR-2* RNAi embryos is due to enhanced PGC migration.

Since a fraction of PGCs die during their active migration to the embryonic gonads, we can assume that the increase in PGCs observed in *sisR-2* RNAi embryos must be a result of a decrease in PGC death (Fig. 1a) [6, 28]. We examined if there was a decrease in PGC death in *sisR-2*

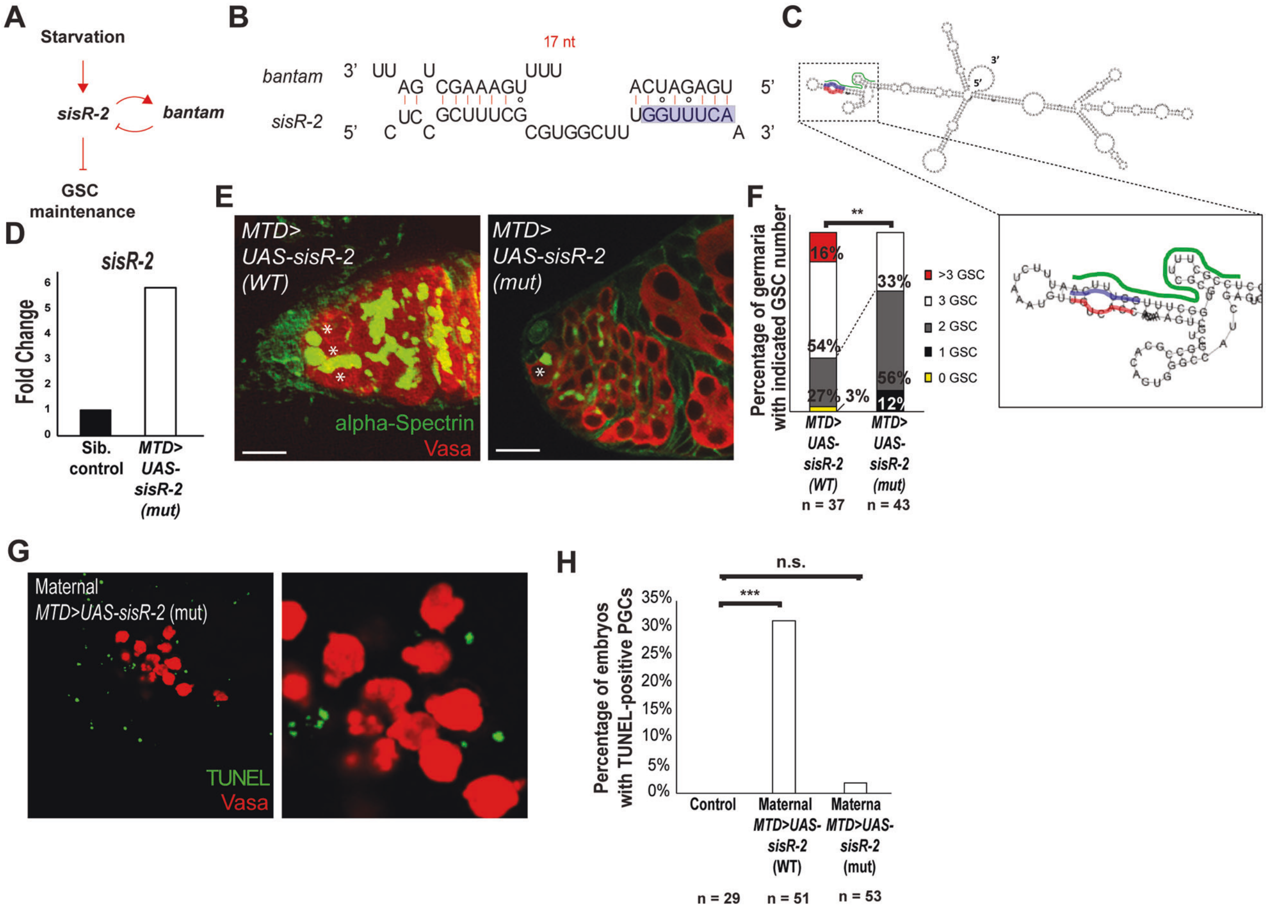

Fig. 2 ***sisR-2* and *bantam* functionally interact. a** Model showing the negative feedback loop between *sisR-2* and *bantam* in regulating GSC maintenance during starvation. **b** Sequence of *bantam* indicating potential stable base-pairing with *sisR-2*. The region mutated to disrupt the seed base-pairing is indicated in blue. **c** Predicted *sisR-2* secondary structure. Green: *bantam* base-pairing region. Blue: mutated nucleotides as indicated in **b**. Red: complementary mutations introduced to preserve *sisR-2* secondary structure. **d** qPCR showing the relative levels of *sisR-2* in ovaries of the indicated genotypes. **e** Confocal images showing the germaria of the indicated genotypes stained with alpha-Spectrin (green) and Vasa (red). GSCs were marked by asterisks (*). **f** Chart showing the percentage of germaria with the indicated number of GSCs in different genotypes shown in **e**. $^{**}p < 0.01$. Fisher's exact test was performed, comparing the percentage of germaria with 2≤ or >2 GSCs. Scale bar: 10 µm. **g** Confocal images showing the PGCs in stage 11 embryos of the indicated genotypes stained with Vasa (red) and TUNEL (green). Panel below is a magnified image of the dashed yellow box. **h** Chart showing the percentage of embryos with TUNEL-positive PGCs of different genotypes shown in **g** and (1 L). The percentage of embryos with TUNEL-positive PGCs in the control (*y w*) and Maternal *MTD > UAS-sisR-2* (WT) first appeared in Fig. 1m. $^{***}p < 0.001$. Fisher's exact test was performed, comparing the number of embryos with or without TUNEL-positive PGCs.

RNAi embryos using TUNEL labeling. However, we were unable to detect TUNEL-positive PGCs even in the control embryos. This is consistent with published literature reporting that it is difficult to detect dying PGCs in wild type embryos [8, 29]. Hence, we wondered if we could instead observe dying PGCs by overexpressing *sisR-2*. Indeed, when we looked for the presence of dying PGCs using TUNEL labeling in stage 11 embryos with increased maternally deposited *sisR-2* (hereafter referred to as *sisR-2* overexpressing embryos) (Fig. S1K and S1L), we were able to detect TUNEL-positive PGCs (0% of control embryos, $n = 29$ vs. 31% of *sisR-2* overexpressing embryos, $n = 51$) (Fig. 1l, m). Furthermore, this increase in TUNEL-positive cells was specific to PGCs as we did not observe an increase in TUNEL-positive somatic cells in the *sisR-2* overexpressing embryos (Fig. S1M). Taken together, our experiments suggest that maternal *sisR-2* promotes PGC death during embryogenesis.

sisR-2 and *bantam* functionally interact

In *Drosophila*, the pro-apoptotic gene *head involution defective (hid)* is zygotically expressed in PGCs and is implicated in PGC death [8, 30]. Interestingly, *hid* is a verified target for the *bantam* miRNA [22]. We previously showed that *bantam* negatively feedbacks and represses *sisR-2* activity to prevent the loss of GSCs during starvation (Fig. 2a) [17]. We speculated that *bantam* represses *sisR-2* activity via a potential 17-nucleotide stable base pairing with *sisR*-2, consisting of a non-canonical seed region containing two G:U wobble base pairs (Fig. 2b, c) [17]. Overexpression of *sisR-2* in the ovaries under fed conditions did not result in a loss of GSCs, possibly due to the repression by *bantam* [17]. To further examine the functional interaction between *sisR-2* and *bantam*, we expressed a mutant form of *sisR-2*, which disrupts the base pairing with *bantam* (Figs. 2b–d, S1L and S2). As expected, overexpression of this mutant form of *sisR-2* in the ovaries resulted in a loss of GSCs (Fig. 2e, f). Hence, this genetic evidence further suggests that *sisR-2* and *bantam* can functionally interact by complementary base-pairing. However, we cannot totally exclude the possibility that the sequence also regulates other targets besides *bantam*. In addition, overexpression of the mutant form of *sisR-2* (*bantam* base-pairing disrupted) no longer resulted in an increase in embryos with TUNEL-positive PGCs as observed in the wild type *sisR-2* overexpression (1.8% of *sisR-2* mutant overexpressing embryos, $n = 53$) (Fig. 2g, h). This experiment suggests that the *bantam* targeting sequence is required to induce cell death in the PGCs.

Maternal *sisR-2* promotes PGC death via *bantam* and *hid*

The *Drosophila* oocyte is transcriptionally quiescent, containing a store of maternally deposited proteins and mature RNAs important for early embryonic development [31]. Like *sisR-2*, *bantam* is also maternally deposited into the oocytes [32]. In transcriptionally active GSCs, *sisR-2* promotes the transcription of *bantam*, while *bantam* targets *sisR-2* to repress its activity [17]. We reasoned that in the oocyte where regulation of RNA occurs only at the post-transcriptional level, the negative feedback loop between *sisR-2* and *bantam* is no longer active (Fig. 3a). Since *sisR-2* and *bantam* can functionally interact via base-pairing, we wondered if the outcome of this interaction could be switched to *sisR-2* inhibiting *bantam* from regulating its target gene(s). To monitor the activity of *bantam* in a *sisR-2* RNAi background, we used a *bantam* sensor transgene [22]. The *bantam* sensor transgene expresses GFP under a tubulin promoter, with two copies of a perfect *bantam* target site in the 3'UTR. Thus, *bantam* activity is reported indirectly through the levels of GFP. Interestingly, we detected a decrease in the levels of GFP in *sisR-2* RNAi ovaries indicating an increase in *bantam* activity (Fig. 3b, c). Because stage 14 oocytes are large, and well-fed flies contain abundant stage 14 oocytes in the ovaries, whole ovaries generally accurately reflect the status of stage 14 oocytes. Thus, our experiment suggests that *sisR-2* acts as a negative regulator of *bantam* activity in the oocytes and early embryos.

Since *hid* is a target of *bantam*, we first examined if expression of *hid* is sufficient to induce PGC death (Fig. 3d). Consistent with a previous report, overexpression of *hid* using the *NGT40* driver led to PGC death (20.9 ± 3.2 PGCs in controls vs. 10.9 ± 3.6 PGCs in *NGT40 > UAS-hid*) (Figs. 3e, f, and S3A) [9]. Furthermore, overexpression of maternal *bantam* led to an increase in PGCs, phenocopying *sisR-2* RNAi (20.9 ± 3.2 PGCs in controls vs. 24.8.3 ± 5.8 PGCs in *MTD > UAS-bantam)* (Figs. 3g, h, and S3B). Next, we hypothesized that *sisR-2* promotes PGC death by inhibiting *bantam* (Fig. 3d). Remarkably, we found that reducing the activity of the maternally deposited *bantam* using a *bantam* sponge transgene could rescue the PGC phenotype in stage 13 *sisR-2* RNAi embryos (32.4 ± 5.3 PGCs in *sisR-2* RNAi vs. 20.4 ± 3.7 PGCs in *sisR-2* RNAi; *bantam* sponge) (Figs. 3g, h, and S4A and S4B). Expression of *bantam* sponge alone had no effect on PGC number, indicating a specific genetic interaction between *sisR-2* and *bantam* (Figs. 3g, h, and S3B). To investigate if *hid* indeed acts downstream of *sisR-2* and *bantam* in the regulation of PGCs, we examined the expression of Hid protein in *sisR-2* RNAi embryos. As expected, Hid protein levels were down-regulated in *sisR-2* RNAi embryos (Fig. 3i, j). Next, we elevated the expression of *hid* in the PGCs of *sisR-2* RNAi embryos. Increase in *hid* expression rescued the PGC phenotype in stage 13 *sisR-2* RNAi embryos, confirming a genetic interaction between *sisR-2* and *hid* (34.4 ± 4.8 PGCs in *sisR-2* RNAi vs. 20.6 ± 6.1 PGCs in *sisR-2* RNAi; *NGT40 > UAS-hid*) (Figs. 3e, f, S4C and S4D). Finally, if *sisR-2* promotes *hid* expression by repressing *bantam*, reducing *sisR-2* is expected to inhibit PGC death by *hid* overexpression. Indeed, *sisR-2* RNAi suppressed the PGC death phenotype caused by *hid* overexpression (10.9 ± 3.6 PGCs in *NGT40 > UAS-hid* vs. 20.6 ± 6.1 PGCs in *sisR-2* RNAi; *NGT40 > UAS-hid*) (Fig. 3e, f).

Maternally deposited *wunen2*, *p53* and *nanos* have been reported to play a role in PGC survival [6–8]. We wondered if *sisR-2* promotes PGC death by regulating the expression any of these three genes as well. Levels of *wunen*2 and *p53* remained unchanged in *sisR-2* RNAi ovaries (Fig. S4E and S4F). Levels of *nanos* also remained unchanged when expression of *sisR-2* was elevated in the ovaries [17]. Thus, it is unlikely that maternal *sisR-2* promotes PGC death by regulating any of these genes. Taken together, maternal *sisR-2* promotes PGC death by inhibiting *bantam* activity, which leads to the derepression of the pro-apoptotic gene *hid* (Fig. 3d).

TOR pathway inhibits *sisR-2* expression

Previously, we have shown that nutritional deprivation promotes the expression of *sisR-2* in the *Drosophila* ovaries [17]. In many organisms, including *Drosophila*, the

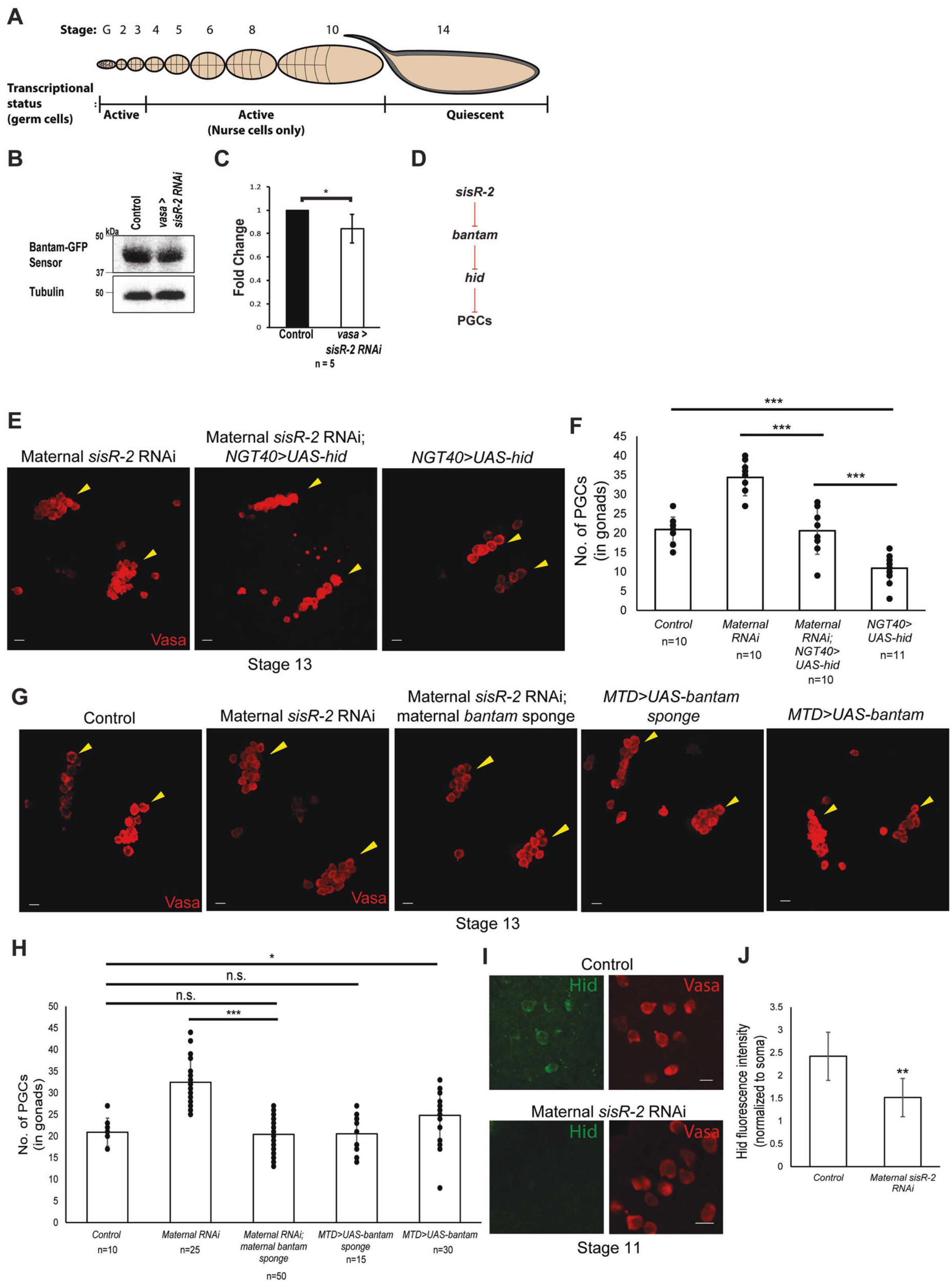

PI3K/AKT signaling pathway is central in mediating changes in nutrition to cellular function [33]. Hence, we hypothesized that this pathway may be involved in regulating *sisR-2* during starvation. During nutrient deprivation, reduced PI3K/AKT signaling results in the inhibition of target of rapamycin (TOR) (Fig. 4a). Thus, we asked

◀ **Fig. 3 Maternal *sisR-2* promotes PGC death via *bantam* and *hid*.** **a** Diagram showing the transcriptional status of germ cells during the different stages of *Drosophila* oogenesis. **b** Western blot showing the level of *bantam*-GFP sensor in ovaries of control and *sisR-2* RNAi flies. **c** Graph showing the relative levels of GFP normalized to Tubulin, as shown in **b**. $*p < 0.05$. Student's *t* test was performed. Error bars depict SD from five biological replicates. **d** Working model. **e, g** Confocal images showing the PGCs in stage 13 embryos of the indicated genotypes stained with Vasa (red). Yellow arrowheads: PGCs in gonads. Maternal *sisR-2* RNAi: *vasa-Gal4* driven RNAi. Maternal *bantam* sponge: *vasa-Gal4* driven *bantam* sponge. **f, h** Charts showing the number of PGCs in the gonads of different genotypes shown in **e** and **g**. Controls in both charts are from the same sample. $*p < 0.05$, $***p < 0.001$. Student's *t* test was performed, comparing the mean number of PGCs of the indicated genotypes. Error bars depict SD. **i** Confocal images showing the PGCs in stage 11 embryos of the indicated genotypes stained with Hid (green) and Vasa (red). **j** Chart showing the relative Hid fluorescence intensity in the PGCs (normalized to soma) shown in **i**. $**p < 0.01$. Student's *t* test was performed. Error bars depict SD from five embryos. Scale bar: 10 µm.

if expression of *sisR-2* is elevated when TOR was inhibited using TOR RNAi. Interestingly, we observed an upregulation of *sisR-2* and its host gene *mushroom bodies tiny (mbt)* in *nos-Gal4 > TOR RNAi* ovaries suggesting that the PI3K/AKT pathway promotes the expression of *sisR-2* via its host gene *mbt* during starvation (Fig. 4a–c).

sisR-2 overexpression induced ectopic division of PGCs

Since starvation promotes the expression of *sisR-2* [17], we wondered if embryos laid by starved female flies exhibit an increase in PGC death. However, starved female flies lay very few eggs, making it technically challenging to collect many staged embryos for the counting of PGCs. Hence, we quantified the number of PGCs in stage 13 *sisR-2* overexpressing embryos. Although embryos with increased maternal *sisR-2* derived from fed mothers is not equivalent to embryos derived from starved mothers, it has been demonstrated that oocytes produced by mothers exposed to these two contrasting nutritional conditions are rather similar [34]. As such, embryos with increased maternal *sisR-2* can likely mirror embryos with starvation induced upregulation of *sisR-2*. We counted the number of PGCs in *sisR-2* overexpressing embryos and did not detect a decrease in the number of PGCs at stage 13 (Figs. 4d, e, S1K and S5A). Instead, we detected a slight increase in PGC number in *sisR-2* overexpressing embryos (Fig. 4e). However, this result was puzzling since we did detect an increase in TUNEL-positive PGCs in stage 11 embryos overexpressing *sisR-2*, which indicated an increase in PGC death (Fig. 1l, m).

During larval development, a decrease in the number of PGCs is corrected by a homeostatic mechanism that involves PGC proliferation [10]. We speculated that although there was an increase in PGC death in the *sisR-2* overexpressing embryos, the inability to observe a decrease in PGCs might be due to ectopic PGC division. Consistent with this idea, we were able to detect the presence of pH3-positive PGCs in stage 12 *sisR-2* overexpressing embryos, indicating that some PGCs were indeed undergoing mitosis (3% in *sisR-2* overexpression vs. 0% in control embryos, $n = 100$) (Fig. 4f). Moreover, this increase in pH3-positive cells was specific to PGCs as we did not observe an increase in pH3-positive somatic cells in the *sisR-2* overexpressing embryos (Fig. S5B). Remarkably, pH3-positive PGCs were not observed in stage 12 embryos overexpressing the mutant form of *sisR-2* suggesting that the effect of *sisR-2* on PGC division also involves *bantam* (Fig. S5C).

bantam represses *brat* in PGCs

From stage 5 till stage 14 of embryogenesis, PGCs are arrested in the G2 phase of the cell cycle [4]. Their transition to mitosis is prevented during migration due to the repression of Cyclin B production by the Nanos/Pumilio translational repressor complex [4, 27]. Overexpression of Cyclin B is sufficient to induce ectopic proliferation of PGCs [4, 27]. In the early embryo, the Nanos/Pumilio complex together with the NHL domain protein Brain tumor (Brat), represses the translation of *hunchback* mRNA to establish posterior patterning of the embryo. The repression of Cyclin B production however does not require Brat [35].

Interestingly, *brat* has been shown to be a target of *bantam* in the *Drosophila* larval brain [36]. Hence, we hypothesized that in the *sisR-2* overexpressing embryos, increase in repression of *bantam* by *sisR-2* might lead to an increase in Brat protein expression in PGCs (Fig. 5a). To examine this, we checked if *bantam* regulates *brat* in the PGCs. Increasing the maternally deposited pool of *bantam* led to a decrease in Brat protein expression (Figs. 5b, c, and S6). Interestingly, this drop in Brat was observed specifically in the PGCs and not in the neighboring somatic cells (Fig. 5b, c). To confirm this observation, decreasing the activity of maternal *bantam* using *bantam* sponge resulted in an increase in Brat protein levels specifically in the PGCs but not in the somatic cells (Fig. 5b, c). Together, these experiments indicate that maternally deposited *bantam* represses *brat* in PGCs (Fig. 5a).

Ectopic Brat expression disrupts *cyclin B* repression

Since Brat interacts with the Nanos/Pumilio complex, we speculated that the increase in Brat in PGCs might interfere with the repression of *cyclin B* by Nanos/Pumilio, resulting in an increase in Cyclin B production and division of PGCs

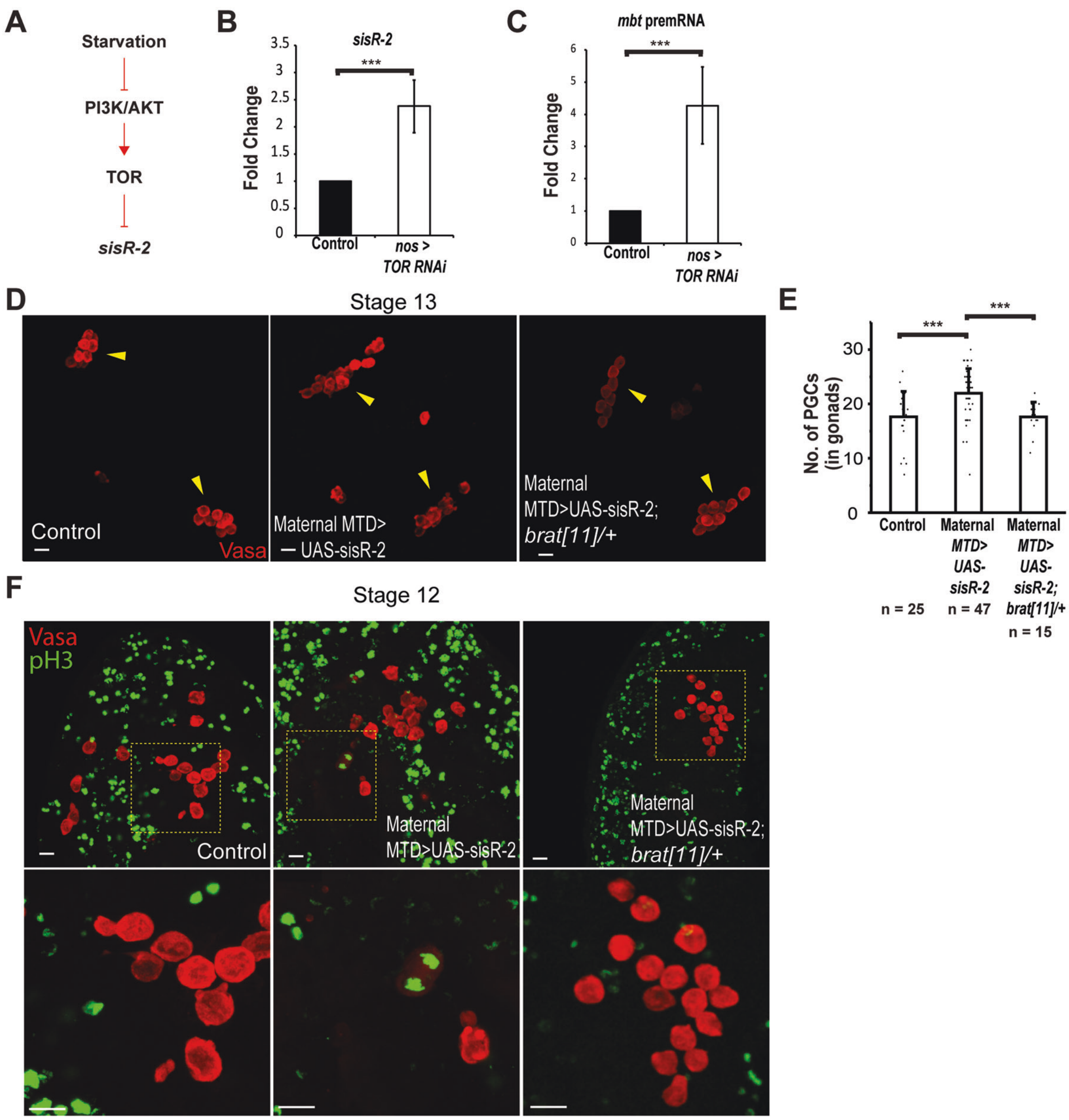

Fig. 4 ***sisR-2*** **overexpression induced ectopic proliferation of PGCs. a** Proposed model. qPCR showing the relative levels of **b** *sisR-2* and **c** *mbt* pre-mRNA in ovaries of the indicated genotypes. $^{***}p < 0.001$. Student's *t* test was performed. Error bars depict SD from three biological replicates. **d** Confocal images showing the PGCs in stage 13 embryos of the indicated genotypes stained with Vasa (red). Yellow arrowheads: PGCs in gonads. Control: *y w*. **e** Chart showing the number of PGCs in the gonads of different genotypes shown in **d**. $^{***}p < 0.001$. Student's *t* test was performed, comparing the mean number of PGCs of the indicated genotypes. Error bars depict SD. **f** Confocal images showing the PGCs in stage 12 embryos of the indicated genotypes stained with Vasa (red) and pH3 (green). Panels below are magnified images of the dashed yellow box. Control: *y w*. Scale bar: 10 μm.

(Fig. 5a). We asked if ectopically expressing Brat in the PGCs can disrupt the repression of *cyclin B* by overexpressing Brat in the embryos using the germline driver MTD-Gal4. Increasing production of Cyclin B eventually results in its shuttling and accumulation into the nucleus, marking the beginning of the progression from the G2 to M phase of the cell cycle [37, 38]. We observed PGCs with accumulation of Cyclin B protein in the nuclei in PGCs from embryos with germline overexpression of Brat, which was not observed in the control embryos (Figs. 6a and S7A). Moreover, germline overexpression of a mutant form of Brat, $Brat^{G774D}$, which has reduced binding ability to Pumilio, did not exhibit nuclear accumulation of Cyclin B protein [35] (Figs. 6a and S7A). This experiment suggests that the binding of Brat to Pumilio is required for the de-repression of Cyclin B production. Thus, these experiments suggest that Brat disrupts the repression of *cyclin B* by the Nanos/Pumilio complex in the PGCs (Fig. 5a).

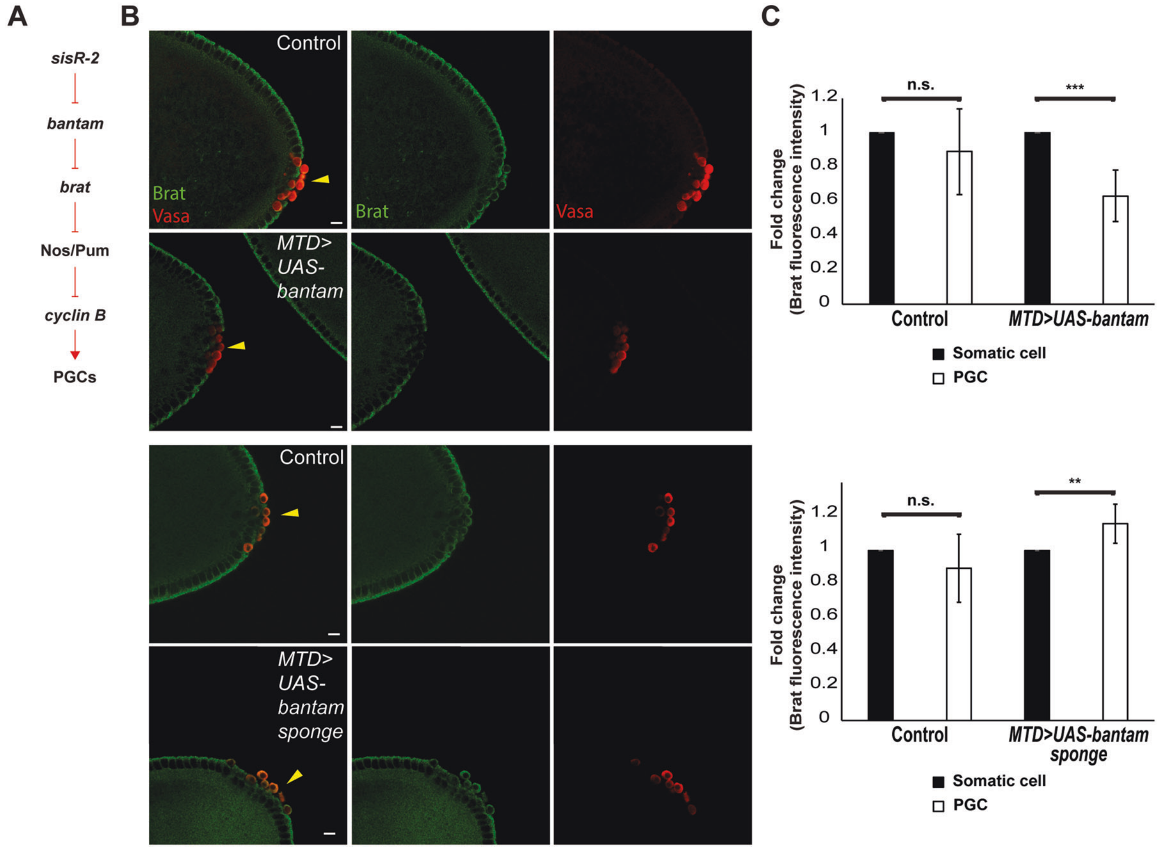

Fig. 5 ***bantam*** **represses** ***brat*** **in PGCs. a** Working model. **b** Confocal images showing the PGCs in stage 5 embryos of the indicated genotypes stained with Vasa (red) and Brat (green). Yellow arrowheads: PGCs at the posterior tip. Control: *y w*. **c** Chart quantifying the Brat fluorescence intensity in PGCs (black bars) and somatic cells (white bars) of the indicated genotypes shown in **b**. $^{**}p < 0.01$, $^{***}p < 0.001$. Student's *t* test was performed. Error bars depict SD from five embryos. Scale bar: 10 µm.

Finally, we asked if Cyclin B protein levels are elevated in *sisR-2* overexpressing embryos. We detected a significant increase in Cyclin B protein in the PGCs of stage 12 *sisR-2* overexpressing embryos as compared to controls (Fig. 6b and c). Furthermore, we also observed PGCs with accumulation of Cyclin B in the nuclei (Fig. S7B). This experiment suggested that the ectopic division of PGCs observed in *sisR-2* overexpressing embryos was due to the de-repression of Cyclin B production. To confirm the role of Brat in the de-repression of Cyclin B production, we reduced one copy of *brat* in the *sisR-2* overexpressing embryos. As expected, we no longer detected an increase in Cyclin B protein levels, as well as the accumulation of Cyclin B in the PGC nuclei (Figs. 6b, c, S7B and S7C). In addition, we were no longer able to detect pH3-positive PGCs in these embryos (Fig. 4f). Finally, the number of PGCs is significantly decreased (17.6 ± 4.6 PGCs in maternal *MTD > sisR-2* vs. 17.6 ± 2.7 PGCs in maternal *MTD > sisR-2; brat[11]/+)* (Fig. 4e). Taken together, our experiments suggest that overexpression of maternal *sisR-2* promotes PGC division via the regulation of Cyclin B through Brat (Fig. 5a).

PGC death and proliferation are independent events

To achieve tissue homeostasis, it is possible that cell death and proliferation are linked. Induction of cell death may trigger proliferation and vice versa. Survival of embryonic PGCs are controlled by cell intrinsic factors [7]. We show that overexpression of *hid* led to a decrease in PGC number (Fig. S3A–C). It was also previously shown that overexpression of Cyclin B led to an increase in PGCs [4]. Thus, induction of cell death or proliferation in PGCs does not trigger a homeostatic mechanism.

We then asked if cell death and proliferation are linked in *sisR-2* overexpressing embryos. If both processes are linked, a decrease in proliferation/death will not lead to a change in PGC number as it is expected to be compensated by a corresponding decrease in death/proliferation. We observed that by reducing *brat*, and consequently proliferation, in *sisR-2* overexpressing embryos, the number of PGCs decreased significantly (Fig. 4e), suggesting that proliferation and death are independent events. We next reduced *hid* in *sisR-2* overexpressing embryos and observed that it did not rescue the proliferation phenotypes as

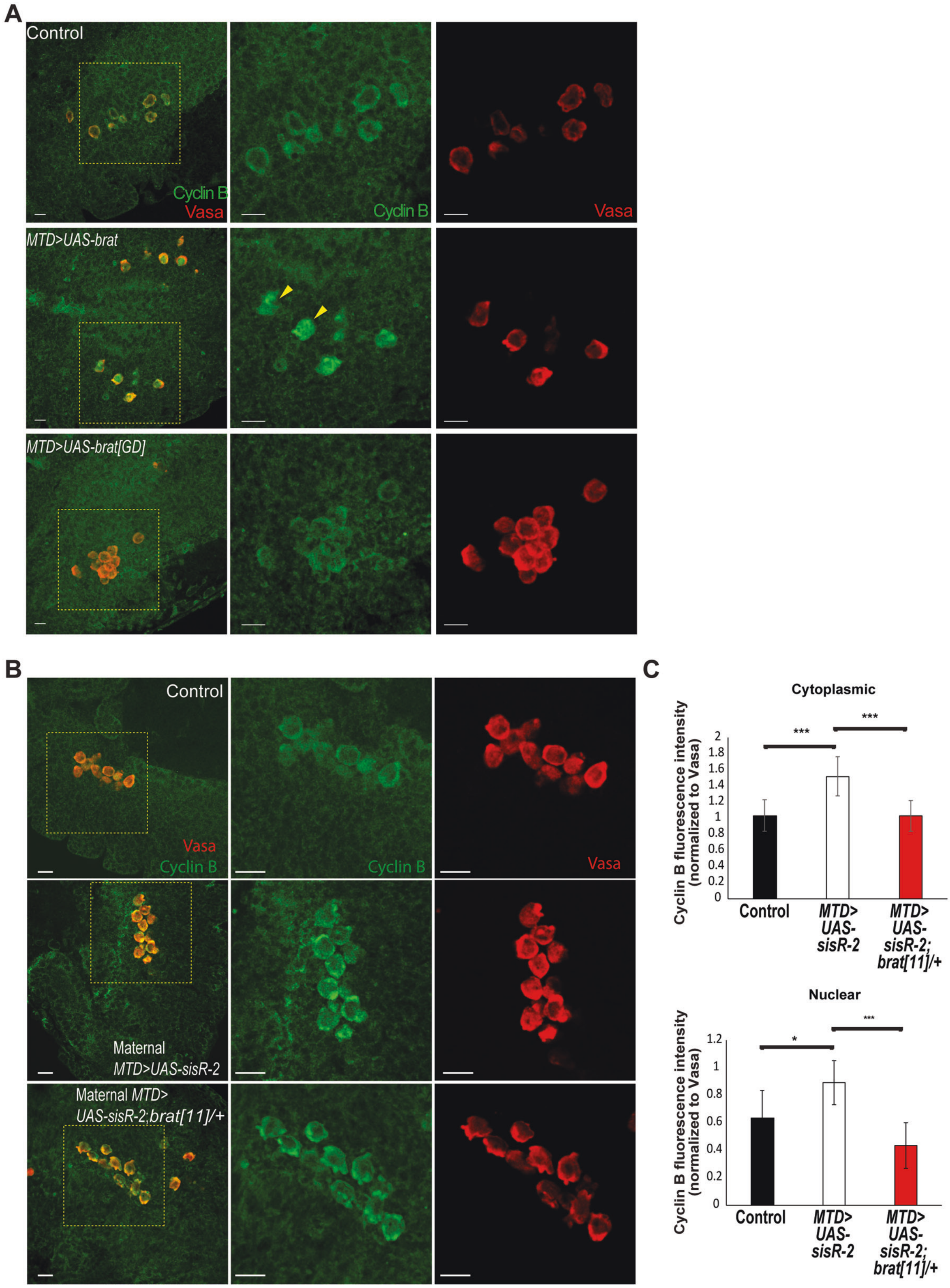

Fig. 6 Ectopic Brat expression disrupts *cyclin B* repression. **a**, **b** Confocal images showing the PGCs in stage 12 embryos of the indicated genotypes stained with Vasa (red) and Cyclin B (green). Panels on the right are magnified images of the dashed yellow box. Yellow arrowheads: PGCs with nuclear translocation of Cyclin B. Control: *y w*. **c** Chart quantifying the Cyclin B fluorescence intensity in PGCs of the indicated genotypes shown in **b**. $***p < 0.001$, $*p < 0.05$. Student's *t* test was performed. Error bars depict SD from five to seven embryos. Scale bar: 10 µm.

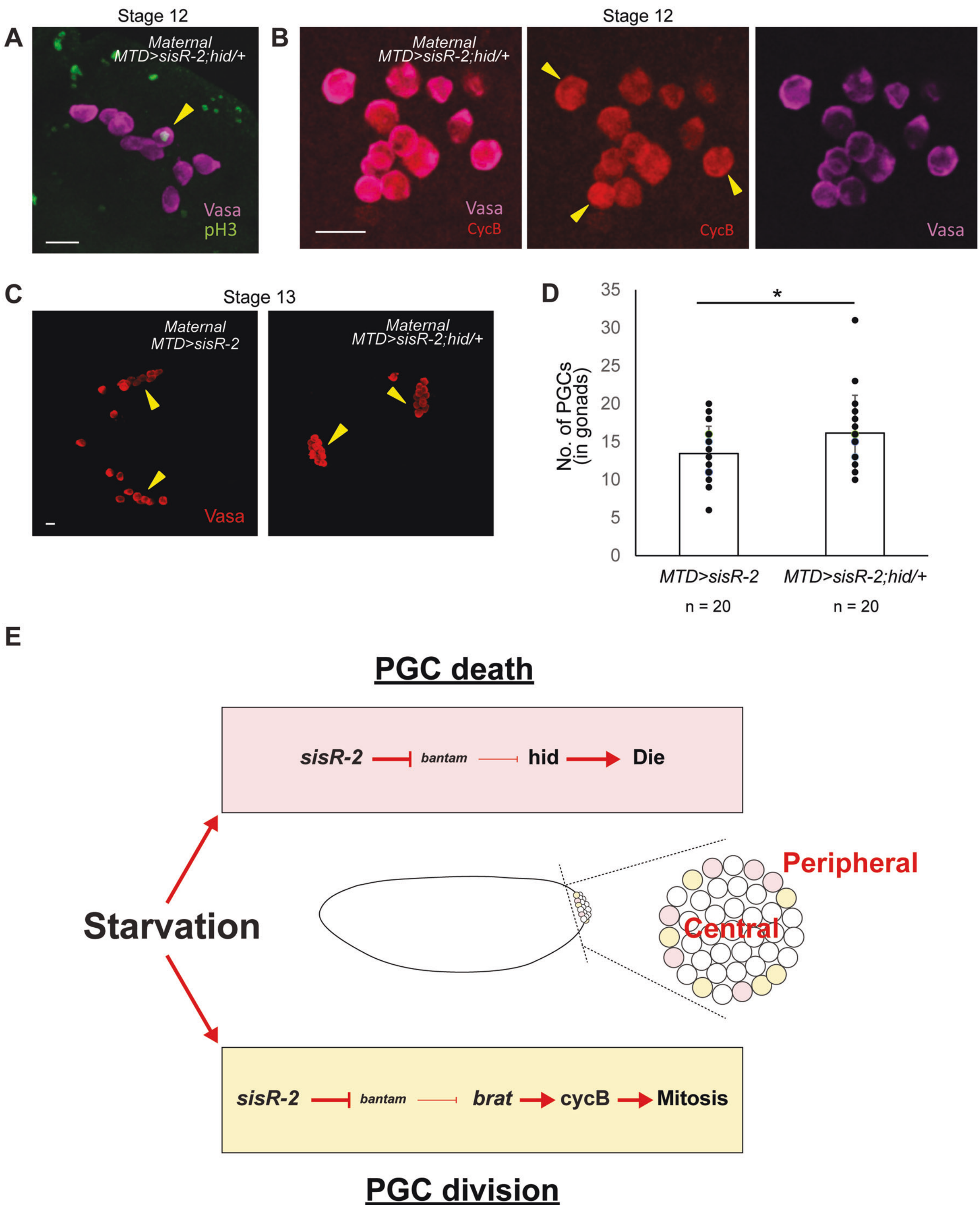

Fig. 7 ***sisR-2*** **coordinates PGC homeostasis via** ***bantam*****. a** A confocal image showing the PGCs in stage 12 embryos of maternal *MTD > sisR-2; hid/+* stained with Vasa (magenta) and pH3 (green). Yellow arrowhead points to pH3-positive PGC. Scale bar: 10 µm. **b** Confocal images showing the PGCs in stage 12 embryos of maternal *MTD > sisR-2; hid/+* stained with Vasa (magenta) and Cyclin B (red). Yellow arrowheads: PGCs with nuclear translocation of Cyclin B. **c** Confocal images showing the PGCs in stage 13 embryos of the indicated genotypes stained with Vasa (red). Yellow arrowheads: PGCs in gonads. **d** Chart showing the number of PGCs in the gonads of different genotypes shown in **c**. $*p < 0.05$. Student's t test was performed, comparing the mean number of PGCs of the indicated genotypes. Error bars depict SD. Scale bar: 10 µm. **e** Proposed model.

indicated by the continued presence of pH3-positive PGCs and nuclear accumulation of Cyclin B (Fig. 7a, b, yellow arrowheads, Fig. S8). Furthermore, it led to a significant increase in PGCs (Fig. 7c, d). Taken together, our experiments suggest that in the embryos, PGC death and proliferation are independent events.

Discussion

In summary, our study reveals a homeostatic mechanism that preserves PGC number during embryogenesis in *Drosophila*. *sisR-2* regulates both PGC death and division by modulating the activity of the miRNA *bantam* (Fig. 7e). We have shown that increasing maternally deposited *sisR-2* results in a drop in *bantam* activity, leading to the derepression of *hid* and an increase in PGC death. Furthermore, a drop in *bantam* activity also leads to the derepression of *brat*, resulting in an increase in Cyclin B production and PGC divisions. How and which population of PGCs make the decision to die or divide remains unclear. Since PGCs formed furthest from the posterior tip (peripheral PGCs) inherit the lowest amounts of germplasm factors such as *nanos* [7], and both *hid* and *cyclin B* are under the translational control of Nanos [8, 27], it is tempting to speculate that peripheral PGCs are likely the most sensitive to changes in *sisR-2* levels (Fig. 7e).

In the *Drosophila* larvae, germline homeostasis is achieved via a non-cell autonomous manner mediated by EGF receptor (EGFR) signaling between the PGCs and the somatic intermingled cells that they are in contact with in the gonads [10]. The mechanism in which germline homeostasis is accomplished during embryogenesis however appears to be different from that during larval development as the embryonic PGCs are not in contact with the SGPs before they reach the gonads. During migration, PGCs are primed or competent to divide during the short window of time. Embryonic PGCs are arrested in the G2 phase of the cell cycle [4] and express the mitosis-promoting cyclin, *cyclin B* [27], however it is translationally repressed during normal conditions. During starvation, although an increase in maternally deposited *sisR-2* promotes PGC death, migrating PGCs can respond quickly by increasing Cyclin B translation and proliferate by entering mitosis.

In the wild, it is reasonable to assume that eggs laid by starved mothers are likely to be in an environment that is deprived of nutrients. Therefore, larvae that hatch from these eggs will be exposed to starvation conditions as well and hence exhibit reduced PI3k/Akt signaling [39]. It has been shown that there is crosstalk between the PI3k/Akt signaling pathway and the EGFR signaling pathway whereby expression of several EGFR pathway components are regulated by the PI3K/AKT pathway [40]. Since larval germline homeostasis is achieved through EGFR signaling, we speculate that this pathway may be impaired in larvae laid by starved mothers. Furthermore, germline knockdown of several PI3K/AKT pathway components resulted in a decrease in PGCs in the larval ovaries [41]. Hence, the embryonic germline homeostatic mechanism identified in this study may be crucial to preserve PGC number during periods of starvation.

Many protective mechanisms to preserve germ cells during nutritional deprivation in adulthood have been previously reported [17, 42, 43]. To the best of our knowledge, this is the first reported example of such a phenomenon occurring in the PGCs during embryonic development. The protective mechanism we uncovered in our study was carried out in flies raised in the laboratory, where starvation may seem like a rather harsh condition to be exposed to in otherwise well-fed animals. However, outside of the well-regulated laboratory, food availability is often limited in the wild [44–46]. Hence, in nature, periodic bouts of starvation might be the norm for most animals. Thus, it is important for animals to have evolved homeostatic mechanisms to preserve their germ cell pool during both development and adulthood to safeguard the survival of their entire species. Therefore, it is very likely that similar homeostatic mechanisms preserving PGCs during embryogenesis are present in other animals as well.

Acknowledgements We thank S. Cohen, H. Ashe, T. Kai, H.D. Ryoo, Y. Yamashita, Developmental Studies Hybridoma Bank, and the Bloomington Stock Center for reagents; K. Okamura, N. Tolwinski, H. Guo, W. C. Liew and members of the Pek lab for discussion. The authors are supported by the Temasek Life Sciences Laboratory.

Author contributions IO conceived the project, performed the experiments and wrote the paper. JWP conceived the project, performed the experiments and wrote the paper.

Compliance with ethical standards

Conflict of interest The authors declare that they have no conflict of interest.

References

1. Donovan PJ. The germ cell–the mother of all stem cells. Int J Dev Biol. 2004;42:1043–50.
2. Mahowald AP. Assembly of the Drosophila germ plasm. Int Rev Cytol. 2001;203:187–213.
3. Sonnenblick B. The early embryogenesis of Drosophila melanogaster. In: Demerec M (ed). Biology of Drosophila (Hafner, New York, 1950). p. 62–163.
4. Su TT, Campbell SD, O'Farrell PH. The cell cycle program in germ cells of theDrosophilaEmbryo. Dev Biol. 1998;196:160–70.
5. Richardson BE, Lehmann R. Mechanisms guiding primordial germ cell migration: strategies from different organisms. Nat Rev Mol Cell Biol. 2010;11:37–49.
6. Yamada Y, Davis KD, Coffman CR. Programmed cell death of primordial germ cells in Drosophila is regulated by p53 and the outsiders monocarboxylate transporter. Development. 2008;135:207–16.

7. Slaidina M, Lehmann R. Quantitative differences in a single maternal factor determine survival probabilities among Drosophila germ cells. Curr Biol. 2017;27:291–7.
8. Sato K, Hayashi Y, Ninomiya Y, Shigenobu S, Arita K, Mukai M, et al. Maternal Nanos represses hid/skl-dependent apoptosis to maintain the germ line in Drosophila embryos. Proc Natl Acad Sci. 2007;104:7455–60.
9. Sano H, Renault AD, Lehmann R. Control of lateral migration and germ cell elimination by the Drosophila melanogaster lipid phosphate phosphatases Wunen and Wunen 2. J Cell Biol. 2005;171:675–83.
10. Gilboa L, Lehmann R. Soma–germline interactions coordinate homeostasis and growth in the Drosophila gonad. Nature. 2006;443:97.
11. Osman I, Tay ML, Pek JW. Stable intronic sequence RNAs (sisRNAs): a new layer of gene regulation. Cell Mol Life Sci. 2016;73:3507–19.
12. Chan SN, Pek JW. Stable intronic sequence RNAs (sisRNAs): an expanding universe. Trends Biochem Sci. 2019;44:258–72.
13. Pek JW. Stable intronic sequence RNAs engage in feedback loops. Trends Genet. 2018;34:330–2.
14. Tay ML, Pek JW. Maternally inherited stable intronic sequence RNA triggers a self-reinforcing feedback loop during development. Curr Biol. 2017;27:1062–7.
15. Wong JT, Akhbar F, Ng AYE, Tay ML-I, Loi GJE, Pek JW. DIP1 modulates stem cell homeostasis in Drosophila through regulation of sisR-1. Nat Commun. 2017;8:759.
16. Pek JW, Osman I, Tay ML, Zheng RT. Stable intronic sequence RNAs have possible regulatory roles in Drosophila melanogaster. J Cell Biol. 2015;211:243–51.
17. Osman I, Pek JW. A sisRNA/miRNA axis prevents loss of germline stem cells during starvation in Drosophila. Stem Cell Rep. 2018;11:4–12.
18. Petrella LN, Smith-Leiker T, Cooley L. The Ovhts polyprotein is cleaved to produce fusome and ring canal proteins required for Drosophila oogenesis. Development. 2007;134:703–12.
19. Van Doren M, Williamson AL, Lehmann R. Regulation of zygotic gene expression in Drosophila primordial germ cells. Curr Biol. 1998;8:243–6.
20. Tracey WD, Ning X, Klingler M, Kramer SG, Gergen JP. Quantitative analysis of gene function in the Drosophila embryo. Genetics. 2000;154:273–84.
21. Ng SSJ, Zheng RT, Osman I, Pek JW. Generation of Drosophila sisRNAs by independent transcription from cognate introns. iScience. 2018;4:68–75.
22. Brennecke J, Hipfner DR, Stark A, Russell RB, Cohen SM. bantam encodes a developmentally regulated microRNA that controls cell proliferation and regulates the proapoptotic gene hid in Drosophila. Cell 2003;113:25–36.
23. Herranz H, Hong X, Cohen SM. Mutual repression by bantam miRNA and Capicua links the EGFR/MAPK and Hippo pathways in growth control. Curr Biol. 2012;22:651–7.
24. Harris RE, Pargett M, Sutcliffe C, Umulis D, Ashe HL. Brat promotes stem cell differentiation via control of a bistable switch that restricts BMP signaling. Dev Cell. 2011;20:72–83.
25. Campos-Ortega JA, Hartenstein V. The embryonic development of Drosophila melanogaster. Berlin: Springer-Verlag; 1985.
26. Patil VS, Kai T. Repression of retroelements in Drosophila germline via piRNA pathway by the Tudor Domain Protein Tejas. Curr Biol. 2010;20:724–30.
27. Asaoka-Taguchi M, Yamada M, Nakamura A, Hanyu K, Kobayashi S. Maternal Pumilio acts together with Nanos in germline development in Drosophila embryos. Nat Cell Biol. 1999;1:431–7.
28. Coffman CR. Cell migration and programmed cell death of Drosophila germ cells. Ann NY Acad Sci. 2003;995:117–26.
29. Hayashi Y, Hayashi M, Kobayashi S. Nanos suppresses somatic cell fate in Drosophila germ line. Proc Natl Acad Sci USA. 2004;101:10338–42.
30. Maezawa T, Arita K, Shigenobu S, Kobayashi S. Expression of the apoptosis inducer gene head involution defective in primordial germ cells of the Drosophila embryo requires eiger, p53, and loki function. Dev Growth Differ. 2009;51:453–61.
31. Spradling A. Developmental genetics of oogenesis. In Bate M, Martinez Arras A (eds). The Development of Drosophila melanogaster (Cold Spring Harbor Laboratory Press, 1993). p. 1–70.
32. Marco A. Selection against maternal microRNA target sites in maternal transcripts. G3 Genes Genomes Genet. 2015;5:2199–207.
33. Hay N. Interplay between FOXO, TOR, and Akt. Biochimica et Biophysica Acta (BBA)-Mol Cell Res. 2011;1813:1965–70.
34. Greenblatt EJ, Obniski R, Mical C, Spradling AC. Prolonged ovarian storage of mature Drosophila oocytes dramatically increases meiotic spindle instability. eLife. 2019;8:e49455.
35. Sonoda J, Wharton RP. Drosophila brain tumor is a translational repressor. Genes Dev. 2001;15:762–73.
36. Weng R, Cohen SM. Control of Drosophila Type I and Type II central brain neuroblast proliferation by bantam microRNA. Development. 2015;142:3713–20.
37. Huang JY, Raff JW. The disappearance of cyclin B at the end of mitosis is regulated spatially in Drosophila cells. EMBO J. 1999;18:2184–95.
38. Ford HL, Pardee AB. Cancer and the cell cycle. J Cell Biochem. 1999;75:166–72.
39. Tettweiler G, Miron M, Jenkins M, Sonenberg N, Lasko PF. Starvation and oxidative stress resistance in Drosophila are mediated through the eIF4E-binding protein, d4E-BP. Genes Dev. 2005;19:1840–3.
40. McNeill H, Craig GM, Bateman JM. Regulation of neurogenesis and epidermal growth factor receptor signaling by the insulin receptor/target of rapamycin pathway in Drosophila. Genetics. 2008;179:843–53.
41. Gancz D, Gilboa L. Insulin and Target of rapamycin signaling orchestrate the development of ovarian niche-stem cell units in Drosophila. Development. 2013;140:4145–54.
42. Angelo G, Van Gilst MR. Starvation protects germline stem cells and extends reproductive longevity in C. elegans. Science. 2009;326:954–8.
43. Wang Y-Y, Sun Y-C, Sun X-F, Cheng S-F, Li B, Zhang X-F, et al. Starvation at birth impairs germ cell cyst breakdown and increases autophagy and apoptosis in mouse oocytes. Cell Death Dis. 2017;8:e2613.
44. Ostfeld RS, Keesing F. Pulsed resources and community dynamics of consumers in terrestrial ecosystems. Trends Ecol Evol. 2000;15:232–7.
45. Markow TA. The natural history of model organisms: the secret lives of Drosophila flies. Elife. 2015;4:e06793.
46. Boulétreau J. Ovarian activity and reproductive potential in a natural population of Drosophila melanogaster. Oecologia. 1978;35:319–42.